



HAL
open science

Dynamics and timescales of mafic–silicic magma interactions at Soufrière Hills Volcano, Montserrat

Rosa Didonna, Fidel Costa, Heather Handley, Simon Turner, Jenni Barclay

► **To cite this version:**

Rosa Didonna, Fidel Costa, Heather Handley, Simon Turner, Jenni Barclay. Dynamics and timescales of mafic–silicic magma interactions at Soufrière Hills Volcano, Montserrat. *Contributions to Mineralogy and Petrology*, 2022, 177 (2), pp.28. <10.1007/s00410-022-01891-z>. <hal-03953746>

HAL Id: hal-03953746

<https://hal.science/hal-03953746v1>

Submitted on 24 Jan 2023

HAL is a multi-disciplinary open access archive for the deposit and dissemination of scientific research documents, whether they are published or not. The documents may come from teaching and research institutions in France or abroad, or from public or private research centers.

L'archive ouverte pluridisciplinaire **HAL**, est destinée au dépôt et à la diffusion de documents scientifiques de niveau recherche, publiés ou non, émanant des établissements d'enseignement et de recherche français ou étrangers, des laboratoires publics ou privés.



HAL Authorization



Dynamics and timescales of mafic–silicic magma interactions at Soufrière Hills Volcano, Montserrat

Rosa Didonna¹ · Fidel Costa^{2,3} · Heather Handley^{1,4} · Simon Turner¹ · Jenni Barclay⁵

Received: 21 September 2020 / Accepted: 12 January 2022
© Crown 2022

Abstract

Mafic magma intrusions into silica-rich magmatic reservoirs are commonly proposed to drive the eruptions of andesitic hybrid magmas that characterise many arc volcanoes. However, interactions between contrasting magmas involve large gradients of physical and chemical properties that change over time, and the details of such processes have proven difficult to constrain. In this paper we investigate the dynamics of magma mingling and mixing using chemical and textural zoning patterns recorded in plagioclase crystals from the February 2010 eruption at Soufrière Hills Volcano, Montserrat. This eruption is considered a classic example of interactions between the andesite magma that constitutes the bulk of the erupted volume and the basaltic andesite that occurs as enclaves. We find that plagioclase crystals are characterised by two well-defined zones that record mafic–silicic magma interaction: a crystal interior, often identified by a patchy, dusty and oscillatory zoning, and an overgrowth zone (rim) of a different composition. We use the anorthite and Mg contents to track the thermal and compositional changes experienced by the crystals over time. Our results reveal that the crystal rims formed a few hours to days prior to eruption, during co-eruptive magmatic interactions. The interaction between the two magmas with contrasting rheology is likely increased by a narrowing conduit geometry towards the surface, which facilitates convection and additional interface contact of the two magmas. Our findings shed new light on the nature and timing of magmatic interactions driving the final eruptive phase at Soufrière Hills Volcano and help to propose an interpretative framework of the monitoring signals.

Keywords Andesite · Enclaves · Mixing · Plagioclase · Diffusion

Introduction

The study of volcanic rocks and their relative composition is a window into the wide range of subvolcanic processes involved in their formation, including mixing of primitive

and evolved magmas, magma source variations, and magmatic differentiation within magma plumbing systems (Edmonds et al. 2019; Holness et al. 2019). For example, the relative efficiency of hybridization (complete mixing) or mingling (physical interactions with incomplete chemical equilibration) varies depending on the range of physical and chemical properties (e.g., temperature, pressure, crystal contents) of the interacting magmas (Spera et al. 1982) and the volume of intruded magma relative to the host (Sparks and Marshall 1986). Macroscopic evidence for mingling and mixing of magma is provided as quenched mafic inclusions in volcanic deposits (Barclay et al. 2010; Browne et al. 2006a; Clynne 1999; Feeley and Dungan 1996; Murphy et al. 1998; Pichavant et al. 2002; Plail et al. 2014). Microscopic mineral textures and chemical zoning patterns in minerals also provide evidence of magmatic interactions (Browne et al. 2006b; Costa et al. 2013b, 2008; Costa and Chakraborty 2004; Costa and Dungan 2005; Kent et al. 2010; Longpre et al. 2014; Tomiya and Takahashi 2005).

Communicated by Timothy L. Grove.

✉ Rosa Didonna
rosa.didonna@mq.edu.au

- ¹ Department of Earth and Environmental Sciences, Macquarie University, Sydney, NSW, Australia
- ² Earth Observatory of Singapore, Nanyang Technological University, Singapore, Singapore
- ³ Asian School of the Environment, Nanyang Technological University, Singapore, Singapore
- ⁴ Department of Applied Earth Sciences (AES), University of Twente, Enschede, The Netherlands
- ⁵ School of Environmental Science, University of East Anglia, Norwich, UK

Many previous studies have provided insights into the varied and complex dynamics that may occur during mafic–silicic magmatic interaction (e.g., Sparks and Marshall 1986; Spera et al. 1982), but the timescales associated to these processes remain difficult to constrain. Volcanic crystals can provide an invaluable insight into the arrival of new mafic magma into a shallow reservoir. Mineral textures and compositions track record pre- and syn-eruptive volcanic processes (Costa and Dungan 2005; Costa et al. 2020; Davidson et al. 2007; Ubide et al. 2021). Many eruptions have been proposed to have been triggered by magma replenishment shortly before eruption (Bacon and Barnes 1978; Clynne 1999; Edmonds and Woods 2018; Eichelberger 1980; Oldenburg et al. 1989; Scaillet et al. 2000; Sparks et al. 1977; Trial and Spera 1990), with replenishment times that can vary from days to weeks (e.g., Devine et al. 2003; Kahl et al. 2013; Kent et al. 2010; Scarlato et al. 2021). In this scenario, longer pre-eruptive timescales (over years) may occur due to the prolonged hybridisation and/or mixing processes of intruded magma that consecutively interacted with the pre-existing magma reservoir, as has been proposed for Merapi (Costa et al. 2013b) and Rabaul volcanoes (Fabbro et al. 2020).

This work aims to investigate the timescales and complex relationship of intrusion–hybridisation–mixing that led to the February 2010 eruption at Soufriere Hills volcano (SHV; Montserrat, Lesser Antilles) (Barclay et al. 1998; Christopher et al. 2014; Devine et al. 1998; Humphreys et al. 2009; Murphy et al. 2000; Wadge et al. 2014). There have been a few studies concerned with the timescales of magmatic processes at SHV. Zellmer et al. (2003b) investigated the magmatic remobilization of the andesite by intruding basalts using Sr and Ba concentration in plagioclase crystals. They found relatively long timescales, on the order of several hundred years. In contrast, Devine et al. (2003) used zoning in Fe–Ti zoning in oxides to study the duration of the thermal excursion on the presumably shallower part of the plumbing system, and reported much shorter timescales, of a few days to weeks. More recently, McGee et al. (2019) used uranium-series data and analysis of $(^{210}\text{Pb}/^{226}\text{Ra})_0$ disequilibria in mafic enclaves and host rocks and found that the mafic enclaves had excess ^{210}Pb . They suggested that input of a deeper volatile component into the shallow plumbing system occurred a few decades before the eruption. Moreover, the input of new volatiles was proposed to have stopped during the final phases of the eruption as revealed by a predominant deficit of ^{210}Pb in the andesite (McGee et al. 2021), which implies that the final eruptions occurred without new mafic magma intrusions in the shallow part of the system.

In this paper, we use the plagioclase textures and compositions, and specially the Mg content as a tracer of mafic melt and model the diffusive re-equilibration of Mg within plagioclase during the final year of the eruption period

(2010). Our results suggest that despite the presence of mafic enclaves throughout the entire eruptive sequence (1995–2010), the Mg-rich mafic magma that intruded in the early stages of the eruption was not necessarily a driver of the eruptive phases until the last year eruption (2010). The short time scales that we report (a few hours or days) rather suggest that mafic magma was already stored in the upper parts of the plumbing systems, and that interactions with silicic melt was facilitated by changes in geometry of the near-surface plumbing system (Gottsmann et al. 2020; Hautmann et al. 2009). Our findings provide new insight into magmatic processes, their timescales and eruption controls at SHV providing additional benefit to the interpretation of monitoring data and the anticipation of future eruptions.

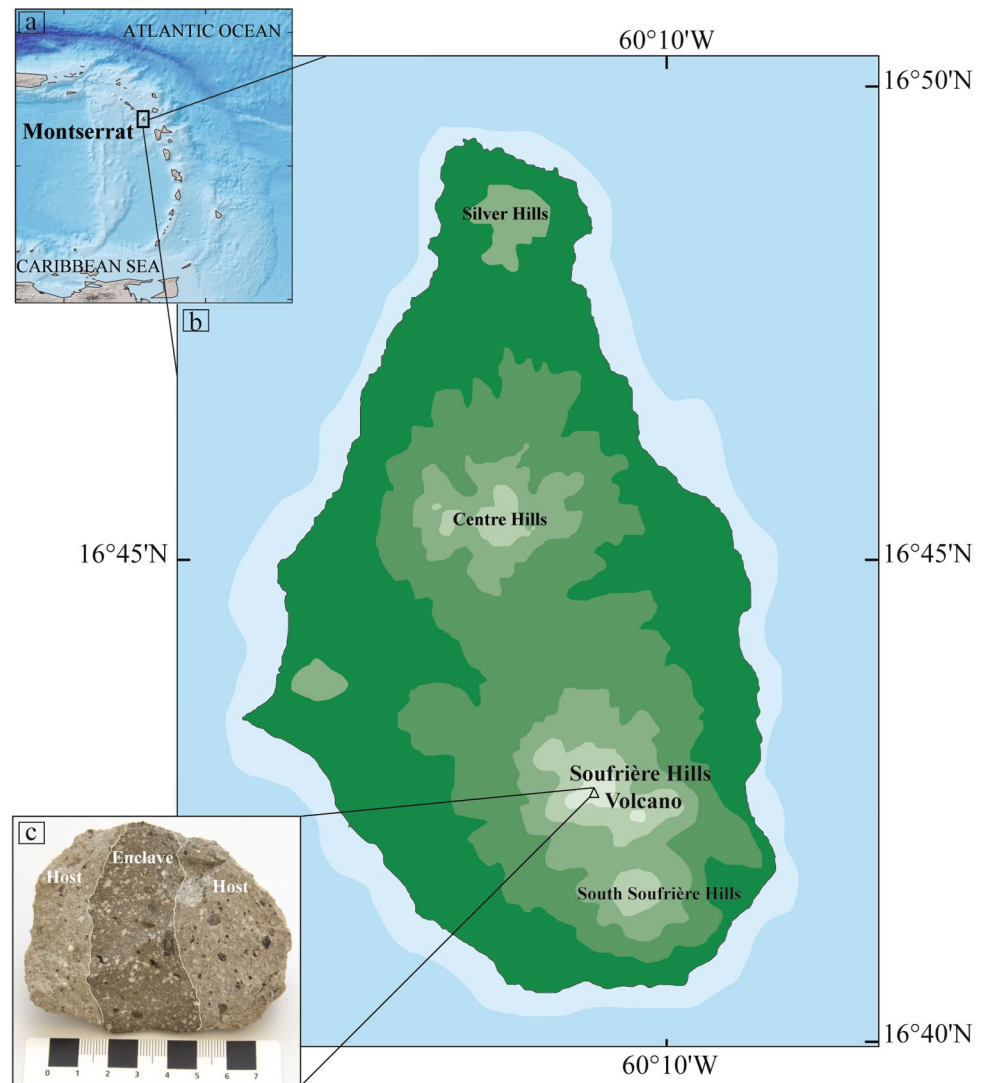
Background of petrology and volcanology of Soufriere Hills Volcano

Soufrière Hills Volcano (SHV) is an island arc volcano located in the southern part of Montserrat Island, Lesser Antilles (Fig. 1a, b). It is comprised of four volcanic centres: Silver Hills (2600–1200 ka), Centre Hills (950–550 ka), South Soufrière Hills volcano (131–128 ka) and SHV proper (282 ka to present) (Coussens et al. 2017; Harford et al. 2002). Andesitic lavas with abundant mafic enclaves are predominant in all of the volcanic centres, except at South Soufrière Hills, which is the only basaltic volcano on the island (Cassidy et al. 2015).

In July 1995, after 3 years of intense seismicity at less than 7 km depth, an eruption started that continued for 15 years, ending in 2010 (Aspinall et al. 1998; Young et al. 1998). The activity of the volcano between 1995 and 2010 is one of the best monitored in the world and has been used as a natural laboratory. The eruption was characterised by episodic lava dome growth and collapse, often accompanied by vulcanian explosive events (Druitt et al. 2012; Ryan et al. 2010; Sparks et al. 2000). Most erupted materials consist of andesitic rocks containing ubiquitous sub-rounded mafic enclaves of several centimetres in diameter (Murphy et al. 2000; Plail et al. 2014). The eruptive period comprises five extrusion Phases (I–V) that differ in the volume of andesitic lava and the proportion of mafic enclaves. Between Phase III and Phases IV and V, the duration of each phase decreased from years to months, while the average extrusion rate increased (Christopher et al. 2014; Wadge et al. 2014).

Previous petrological studies found that the andesite is phenocryst-rich (33–63 vol%), with a phenocryst assemblage composed of plagioclase (64–78 vol%), amphibole (8–28 vol%), orthopyroxene (3–7 vol%), microphenocrysts of Fe–Ti oxides (1.5–3 vol%) and clinopyroxene (< 1 vol%) with minor quartz (sometimes embayed by clinopyroxene rim). The groundmass of the andesite is also typically

Fig. 1 **a** Location map of Montserrat Island in the Caribbean Sea. **b** Simplified map of Soufrière Hills volcano showing the location of the Soufrière Hills vent (black triangle). **c** Photograph of rock sample (MT35) used in this study that was collected from deposits of the dome collapse (11 February 2010). Andesite (light grey) and basaltic andesite (dark grey band in the centre)



crystal-rich and includes up to 25% rhyolitic glass (Christopher et al. 2014). Andesite textures, modal proportion and mineral composition do not change significantly from Phase I (Murphy et al. 2000) to Phase III (Humphreys et al. 2009; Christopher et al. 2014). Although the volcanic activity of Phase IV and V changed compared to the first three phases, the andesite characteristics remained invariable (Christopher et al. 2014). The mafic enclaves contain a similar mineral assemblage to the andesite, of predominantly mafic minerals with clinopyroxene more abundant than orthopyroxene. Many of the crystals in the enclaves have been interpreted as xenocrysts derived from the andesite host (Christopher et al. 2014; Humphreys et al. 2009).

A detailed description of the enclaves are provided by Plail et al. (2014) who subdivided the enclaves from rocks erupted during Phase IV and V in three types (A, B and C) according to the degree of interaction between the andesite

and the more mafic magma. Type A enclaves are the most basaltic in composition, containing a few inherited phenocrysts and a narrow compositional range in whole rock. The Type A enclaves are characterised by chilled margins, high-Al amphibole and high vesicularity. Type B enclaves show a broader compositional range (basaltic andesite), with numerous inherited phenocrysts, lack of chilled margins, low vesicularity and rare high-Al amphibole. Finally, Type C enclaves are composite, with a mafic interior (Type A) and hybrid exterior (Type B) representing an interface between the two types. It is noteworthy that the proportion of mafic enclaves appears to increase throughout the eruptive period, from ~1% volume of the erupted material in Phase I (1997), to approximately 5–7% volume in Phase IV, and 3–8% volume in Phase V (Barclay et al. 2010; Komorowski et al. 2010; Murphy et al. 2000; Plail et al. 2014).

Samples and methods

Sample description

We used a sample that included andesite host and enclave material (MT35; Fig. 1c) collected by Plail (2013) from deposits of the dome collapse generated on 11 February 2010 (Phase V) and representative of the most basaltic enclave type (Type A). The andesite bulk-rock composition (60.5 wt% SiO₂, 2.6 wt% MgO) is more evolved than the mafic enclave, which is basaltic andesite with 52 wt% SiO₂ and 4.8 wt% MgO (Fig. 2; Plail 2013). The major element composition of the enclave in MT35 lies towards the more mafic end of the compositional range characterising the SHV enclaves (49–56 wt% SiO₂ and 3.5–5.5 wt% MgO).

Analytical methods

We investigated ten polished sections (30 and 100 μm in thickness) of sample MT35 [MT1 (a, b, c, d), MT2 (e, f, g), and MT3 (h, i, m)]. Optical microscopy was used to identify the main textural and mineralogical features of both the host andesite and the enclave. Backscattered electron (BSE) images of 24 plagioclase minerals were obtained using a Zeiss EVO MA15 scanning electron microscope with an accelerating voltage of 15 kV at Macquarie University

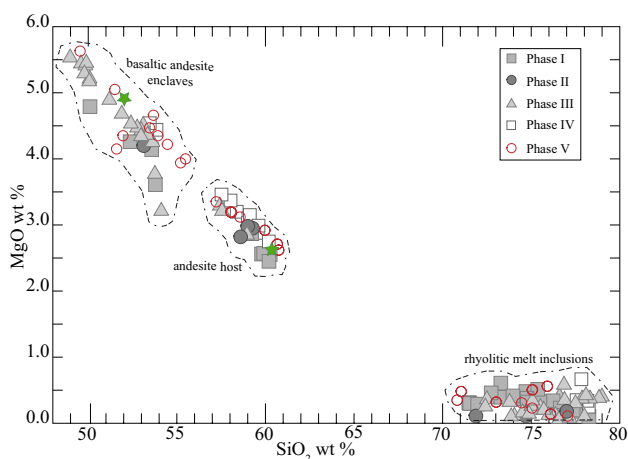


Fig. 2 MgO vs SiO₂ contents of andesite host rock and basaltic andesite enclaves of the five phases of extrusive activity from 1995 to 2010 at SHV: Phase I (Barclay et al. 1998; Christopher et al. 2014; Devine and Rutherford 2014; Zellmer et al. 2003a; Mann 2010); Phase II (Christopher et al. 2014; Humphreys et al. 2010; Mann 2010); Phase III and IV (Christopher et al. 2014; Humphreys et al. 2010; Plail et al. 2014); Phase V (Christopher et al. 2014; Devine and Rutherford 2014; Plail 2013). Rhyolitic melt inclusions compositions are also displayed (from Christopher et al. 2014; Devine and Rutherford 2014; Plail 2013). Green stars represent the bulk-rock compositions of sample MT35 studied in this work

(Sydney, Australia). Brightness and contrast were varied to accentuate the textures. A large BSE image of the MT2e slide (resolution 5256 × 12,236 pixels) was acquired with the JSM-7800F Field Emission Scanning Electron Microscope at Nanyang Technological University (NTU, Singapore) using a super hybrid lens (SHL) which provided an excellent resolution of 0.8 nm at 15 kV (Fig. 3). Modal proportions of mineral phases were obtained by analysing the MT2e large image with the “ImageJ” program.

Quantitative analyses were performed using a JEOL JXA 8530F field emission Electron Probe MicroAnalyzer (EPMA) at NTU. The operating conditions for plagioclase were an accelerating voltage of 15 kV, a beam current of 10 nA for Si, Al, Ca, Na, K, Fe (ka) and 80 nA for P,

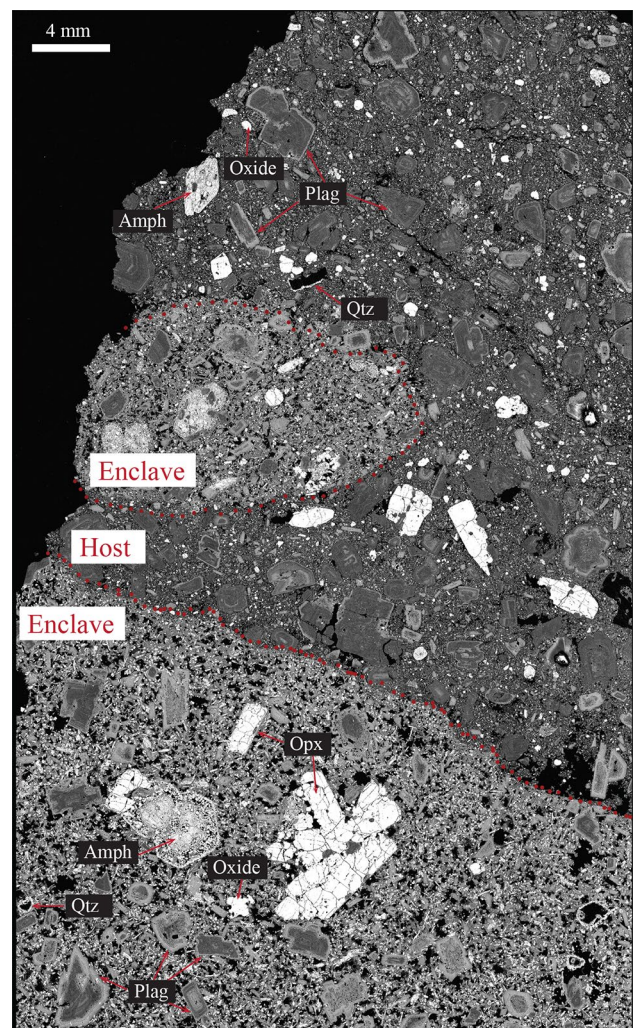


Fig. 3 Backscattered electron (BSE) image of section MT2E that includes andesite (Host) and basaltic andesite enclaves (Enclave). Strongly zoned plagioclase crystals (shown by the large and abrupt difference in grey scale between crystal cores and rims) also have a sieved-textured zone. Quartz typically has a reaction rim of clinopyroxene. Amphibole in the enclave displays a reaction rim, whereas amphibole reaction rims are absent in the andesite

Mg, Ti, Mn (ka) and with a focussed beam. The standards used were Plagioclase (Astimex block) for Al and Ca (ka); Apatite for P (ka); Albite for Na and Si (ka); Rutile for Ti (ka); and Specularite for Fe (ka) and Orthoclase. Counting times were set to 10 s (Na), 20 (Al and Si), 30 s (Ca), 40 s (K, Fe and Mn), and 80 s (Mg, Ti and P) ka. Increased counting times were used to increase counting statistics for elements with lower concentrations and the goodness of the analyses were checked with structural formula calculations. High-resolution profiles of approximately 1 μm (μm) spacing were obtained across compositional gradients in plagioclase as identified by grayscale changes in the BSE images. Although such close analytical spacing may lead to convolution effects in the profiles (Morgan et al. 2004), it provides a way to calculate the maximum timescales via diffusion modelling (see “Modelling” section). The EPMA traverses were obtained perpendicular to one of the crystal margins and far from crystal corners to avoid artefacts of diffusion along multiple dimensions or skewed lengths of the gradient (e.g., Costa et al. 2003, 2008). The two and three-dimensional re-equilibration effects were mitigated by focusing only on profiles with large compositional profiles. The EPMA traverses were carried out to determine the compositional boundary between the rim and interior zones, as identified by grey scale changes in the BSE images. High-resolution EPMA traverses were not conducted for patchy and sieve-textured crystal cores due to the abundance of mineral and/or melt inclusions.

Compositional traverses of plagioclase were obtained from section MT2e, which was selected as representative of the different plagioclase textures. In total, 21 plagioclase crystals were analysed: 12 from the host (~1000 data points) and 9 from the enclave (~800 data points). Mineral abbreviations and end-members are used as follow: amphibole = amph, orthopyroxene = opx, quartz = qtz, clinopyroxene = cpx, Anorthite content as %An = $100 \times \text{molar Ca}/(\text{Na} + \text{Ca} + \text{K})$, Mg-number [Mg# = $100 \times \text{molar Mg}/(\text{Mg} + \text{Fe}^*)$, where Fe* = is total iron] (Deer et al. 1992).

Modelling

We focussed on modelling the re-equilibration of Mg concentration of plagioclase phenocrysts that have large and abrupt changes in An content, as these provided well-defined initial conditions and An diffuses many orders of magnitude slower than Mg at the same temperature (Grove et al. 1984). We used an equation that takes into account the dependence of the partitioning and diffusivity on anorthite composition and temperature (Costa et al. 2003). The following parameters and assumptions were used in the modelling (see Supplementary Information for more details):

1. During magma mixing events, plagioclase crystals experienced significant changes in temperature and composition over time, therefore, it is difficult to associate a given plagioclase composition with a unique temperature and melt composition. Previous estimates of the andesite host temperature obtained with geothermobarometry and in experimental studies range from 850 ± 20 °C (Supplementary Table S1; Barclay et al. 1998; Christopher et al. 2014; Devine et al. 1998, 2003; Devine and Rutherford 2014; Humphreys et al. 2009; Murphy et al. 1998, 2000) up to 1000 °C (Supplementary Table S1; Christopher et al. 2014; Humphreys et al. 2009; Murphy et al. 1998, 2000). The temperature variation of the mafic magma within the enclave is likely to have been large, up to 1100 °C (Christopher et al. 2014; Humphreys et al. 2009; Plail 2013). Thus, for the estimation of melt composition and diffusion modelling, we explored a temperature range of 850–1100 °C (± 50). We used different Mg initial and equilibrium profiles (Summary in Supplementary Table S2) depending on the anorthite content and on their relative temperature (950 °C for plagioclase in the host and 1050 °C found in the enclave).
2. Partition coefficients between plagioclase and melt available in the literature have been obtained using different temperatures, pressures and/or melt compositions (Bindeman et al. 1998; Blundy and Wood 1991; Dohmen and Blundy 2014; Putirka 2005). We calculated the melt Mg compositions in equilibrium with the plagioclase using Eq. (2) in Bindeman et al. (1998), which is dependent on An content and temperature. Results were compared with values obtained using the formulation proposed by Dohmen and Blundy (2014) with more input variables such as temperature, An molar fraction in plagioclase and SiO₂ content in the melt (see Supplementary Information for more details).
3. We used the diffusion coefficient for Mg in the plagioclase of Van Orman et al. (2014), which depends on the An content and temperature.
4. Diffusion modelling of Mg was carried out in one dimension using Eq. (7) in Costa et al. (2003) and solved numerically by finite differences coded in Matlab[®]. A step change in Mg was used for the initial conditions, following the change of each individual crystal. The rim of the crystal is considered as an open boundary in equilibrium with a fixed melt composition. The best match between data and model was determined by minimising the root mean square (rms) of the differences between fit-computed and measured profiles within the relative uncertainty obtained from EPMA instruments. Given the geometry of the crystals and the shape of the concentration profiles, we ran one- and two-stage models (e.g., Drituit et al. 2012) to compute the diffusion timescales.

The one-stage models assume that the entire plagioclase rim grew quickly and then re-equilibrated with its interior. The two-stage models account for a more realistic situation in which the plagioclase crystals experience an episode of re-equilibration with a liquid prior to rim formation. Thus, the two-stage models comprise a first step in which the Mg concentration in the interior part of plagioclase re-equilibrate directly with a liquid (Step 1, interior-boundary transition), and a second step in which the rim grows quickly and the diffusion occurs through the entire crystal (Step 2, interior-rim). This approach has already been successfully used in other volcanic systems (Druitt et al. 2012; Fabbro et al. 2017; Flaherty et al. 2018).

Results

General petrographical and textural observations

The andesite sample is crystal-rich (32 vol% phenocrysts), dominated by plagioclase (87%), orthopyroxene (8%), amphibole (2%), Fe–Ti oxides (3%) and minor quartz (<1%) (Supplementary Table S3). Plagioclase is the most abundant mineral in the groundmass and exhibits a range in sizes that gives a seriate texture. The groundmass contains microlites of orthopyroxene (opx), clinopyroxene (cpx), Fe–Ti oxides and glass, with almost no vesicles. Plagioclase displays a variety of textures and zoning patterns, described in the next section. Single opx phenocrysts (crystals > 300 μm) are unzoned or have a thin rim (< 10 μm) of cpx. Amphibole (amph) shows evidence of reaction textures made of other minerals, and some crystals contain inclusions of plagioclase and oxides. Quartz (qtz) has reaction rims of cpx and magnetite, apatite and rare zircon are also present (Fig. 3). The sample has similar mineralogy and crystal content to that described of previous SHV eruptions (e.g., Christopher et al. 2014; Couch et al. 2001; Devine et al. 1998; Humphreys et al. 2009, 2010; Murphy et al. 1998, 2000).

The enclave is a basaltic andesite (20 vol% phenocrysts) and contains the same mineral assemblage as the host andesite (Supplementary Table S3), with plagioclase (65%), amphibole (20%), orthopyroxene (15%), Fe–Ti oxides (<1%), and minor quartz (<1%). The enclave shows more developed and pronounced mineral reaction textures than the andesite (Fig. 3). Phenocrysts of opx occur as single isolated grains or as glomerocrysts (up to 8 mm in length), with reaction rims of cpx and can be unzoned or reversely zoned (i.e., higher Mg/Fe in the rims than in cores). Large reacted amph, qtz and Fe–Ti oxides are more abundant in the enclave than in the host. Amph crystals (up to 5 mm in size) show reaction rims of cpx, plagioclase, oxides and/or glass. Phenocrysts of qtz, with or without reaction rims

of cpx (up to 2 mm in size) are also present. Magnetite is more abundant than ilmenite and can be found with a rim of ilmenite. Accessory minerals are apatite and rare zircon. The groundmass of the enclave contains euhedral thin laths of plagioclase, amphibole and pyroxenes as well as vesicles that are bounded by crystals with margins that are indicative of fast quenching (Fig. 3). These are also similar abundances and mineralogy as reported in previous studies (e.g., Plail et al. 2014; Mann 2010).

Plagioclase textures and zoning patterns

Plagioclase occurs as phenocrysts (up to ~4 mm in size), microphenocrysts (100–300 μm), and microlites (< 100 μm) and exhibits a wide range of textures and compositions in both the host (andesitic) and in the enclave (basaltic andesite; Fig. 3). We note that here we use the term phenocryst for designating the size, rather than the origin (e.g., xenocrysts) of the crystals (Davidson et al. 2007). We initially identified plagioclase core, intermediate and rim zones using the greyscale changes from high-resolution BSE images (Fig. 3) and later confirmed the textural boundaries by quantitative compositional profiles across the various plagioclase zones. However, given the abundant dissolution surfaces, patchy zoning, minerals inclusion and resorption zones of many plagioclase cores, we did not attempt to obtain quantitative traverses as these could not be used in our Mg-modelling. We classified the plagioclase crystals into two main types (I and II) using An, Mg and Fe profiles from rim to intermediate-core zones (Fig. 4).

Type I plagioclase are mainly found in the host (90 vol%; 10 vol% in the enclave) and tend to be euhedral in shape (Fig. 5). They are reversely zoned in An, with a high An rim (up to An₆₅), surrounding an intermediate-core zone of

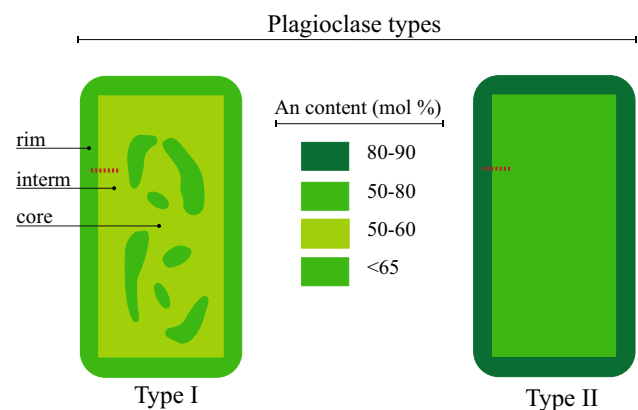


Fig. 4 Schematic representation of plagioclase types I and II based on anorthite (An) content. Chemical analysis and diffusion modelling were performed across the transition rim and intermediate-core zones (red dotted line)

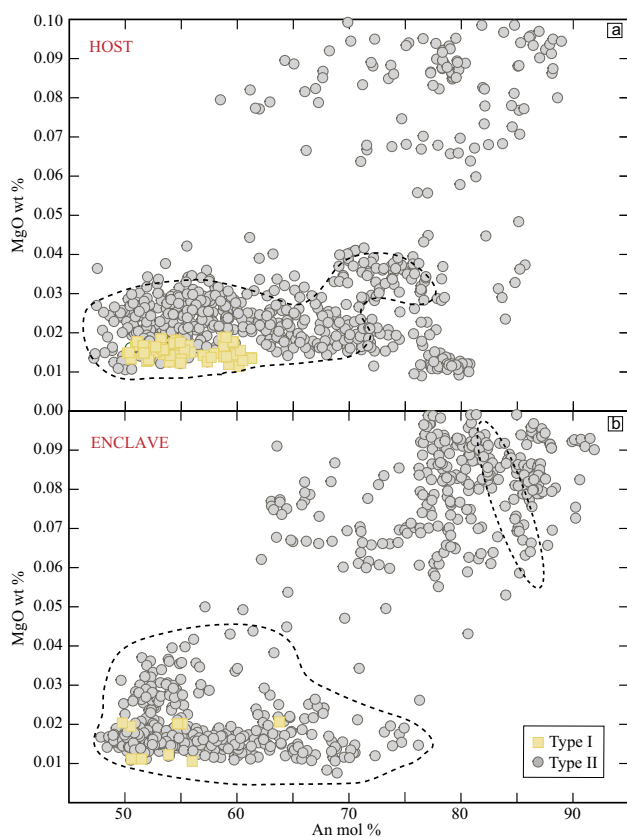


Fig. 5 Anorthite vs MgO content in plagioclase phenocrysts, within host **a** and enclave **b**, according to type I and II classification. Fields denoted by dashed lines indicate the intermediate-core zones of plagioclase crystals. Note that the compositional ranges of host and enclave tend to overlap, although the population of high An and MgO (intermediate-core zones of type II), which occurs in the enclave has not been found in the host (see main text for details)

lower An (50–60 mol%) and patchy zoning. Compositional traverses show that Mg and Fe contents co-vary with An content in plagioclase in both the host (Fig. 6) and enclave (Fig. 7). Rim to intermediate-core traverses show that many Type I plagioclase have positively correlated An and MgO concentrations (H6 in the host, Fig. 6), but An is less well correlated with FeO*. At the boundary between the rim and intermediate-core, changes in An content are sharp and occur within $< 5 \mu\text{m}$, while variation in MgO content at the boundary is not significant at the boundary, varying $< 0.02 \text{ wt}\%$.

Type II plagioclase crystals are primarily found in the enclave (70 vol%; 30 vol% in the host) and show reverse zoning patterns, with a high An rim (up to 90 mol%) that surrounds anhedral and sub-rounded intermediate-core zones (An_{50-70} ; Figs. 4, 5). Some type II plagioclase crystals found only in the enclave display an intermediate-core with high An ($> 80 \text{ mol}\%$) and high Mg ($> 0.06 \text{ wt}\%$; Fig. 5b). The transition between rim and intermediate-core zone is

abrupt, commonly occurring over distances $< 5 \mu\text{m}$ (Figs. 6, 7). Changes in MgO content are sharp and larger compared with type I (up to 0.1 wt%). Type II plagioclase shows complex textures, with sieve-textures, dissolution surfaces and resorption zones.

The classification of our type I and II is in general consistent with previous classifications by Murphy et al. (2000) and Plail et al. (2014). Based on mineralogical textures and An content, our type I crystals are similar to the type 2 crystals in the andesite host of Murphy et al. (2000), with reversely zoned phenocrysts with cores typically sodic (An_{48-58}) and rims with An_{65-80} . Following Plail et al. (2014) and Murphy et al. (2000), reverse zoned dusty sieve-textured plagioclase crystals (type 2 and type 3, respectively) are comparable to our type II found in host and enclave. Although most type II crystals have high calcic outer rims (e.g., E2, H11), some are more sodic, with An 55–65 (e.g., E1, H10) comparable to type 3 crystals of Murphy et al. (2000). Our classification is inline with the distinction proposed by McGee et al. (2021), between “older” plagioclase crystals, with sieve texture and complex oscillatory zoning, and “younger” plagioclase crystals, lacking in sieve texture. McGee et al. (2021) identified plagioclase crystals with excess or deficit of Pb, and found that “younger” crystals are characterised by higher $(^{210}\text{Pb}/^{226}\text{Ra})_0$ ratios and higher equilibrium $(^{210}\text{Pb}/^{226}\text{Ra})_0$ ratios than “older” plagioclase, basing their classification on the fact that partition coefficients for Pb in plagioclase crystals are higher than those for Ra in plagioclase crystals.

Estimation of melt compositions in equilibrium with host and enclave

The calculated melt MgO contents in equilibrium with rim and intermediate-cores of type I crystals are $< 2 \text{ wt}\%$ (at $T = 850\text{--}1100 \text{ }^\circ\text{C}$; Fig. 8) and $\text{An} < 65 \text{ (mol}\%)$ for those from host and enclave. Instead, for type II plagioclase, rims and intermediate-core zones are in equilibrium with diverse melt MgO and An contents. For example, in the host, type II intermediate-core zones with An content up to 70 (mol%) are yielded Mg content up to 2 wt% (at $850 \text{ }^\circ\text{C}$; Fig. 8a) and $\text{MgO} < 1 \text{ wt}\%$ (at $1100 \text{ }^\circ\text{C}$; Fig. 8e). Instead, in the enclave, plagioclase with An lower than 60 mol% show lower MgO concentration ($< 1 \text{ wt}\%$; at $850\text{--}1100 \text{ }^\circ\text{C}$; Fig. 8 b, d, f) than plagioclase intermediate-core zones with higher An (65–75 mol%) that are re-equilibrated with higher MgO content of 2–6 wt% for melts at $850 \text{ }^\circ\text{C}$ (Fig. 8b) and $\text{MgO} < 3 \text{ wt}\%$ for melts at $1100 \text{ }^\circ\text{C}$ (Fig. 8f).

The rims of type II plagioclase are in equilibrium with melt at $850 \text{ }^\circ\text{C}$ and MgO contents $> 1 \text{ wt}\%$ for the host (Fig. 8a) and $\text{MgO} > 6 \text{ wt}\%$ for plagioclase from the enclave (Fig. 8b). For higher melt temperatures (e.g., $1000 \text{ }^\circ\text{C}$), rims in the host show lower MgO content (1–3 wt%; Fig. 8c) compared to those from the enclave

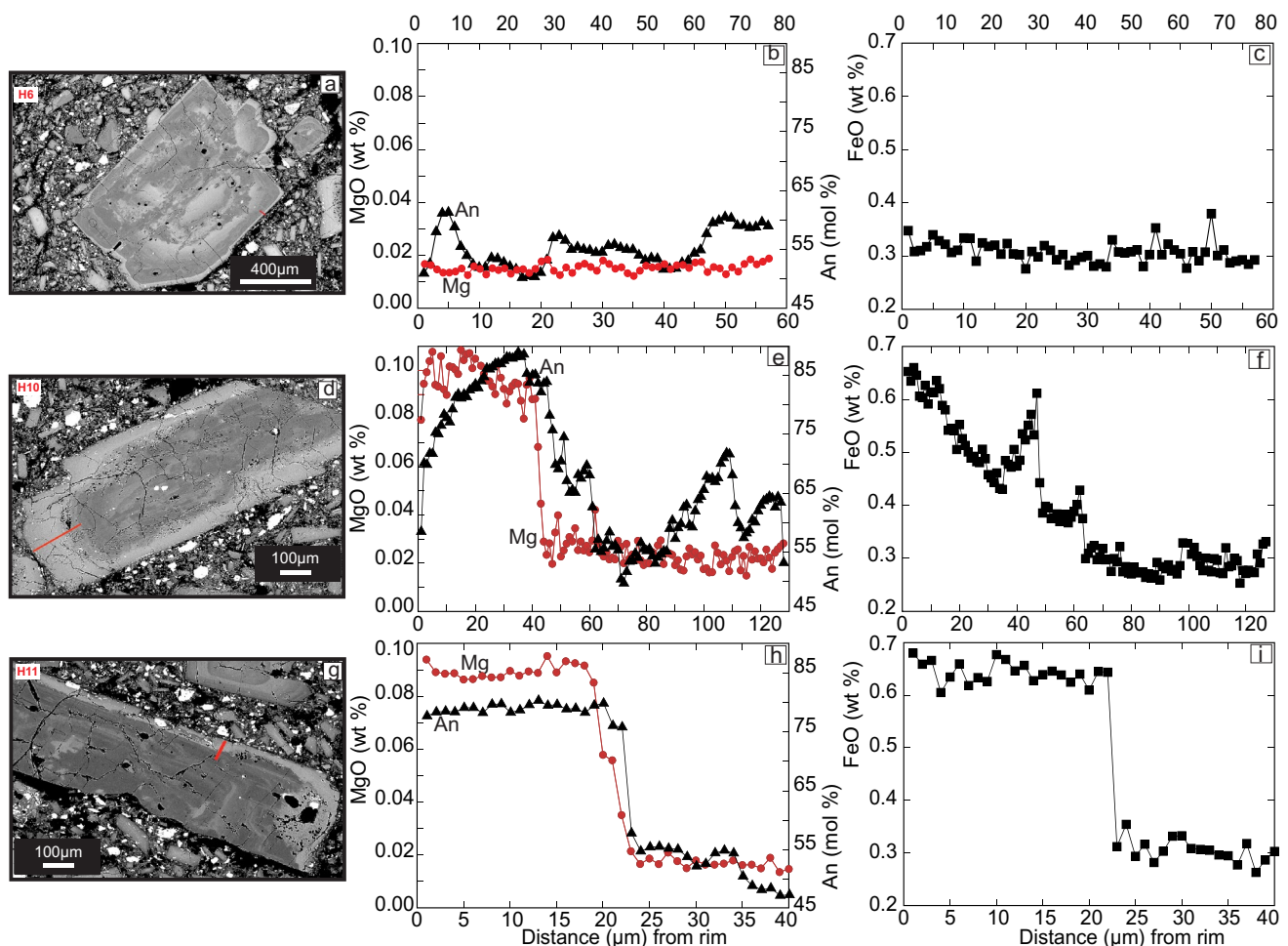


Fig. 6 Examples of BSE images and compositional traverses of type II plagioclase from the enclave. Red lines mark the position of the electron microprobe traverse. E1 **a**, E2 **d** and E9 **g**. Crystals show patchy cores, with a sharp increase in An (black triangle), MgO (red

circle) and FeO content (black square) at the boundary between the rim and the crystal intermediate-core (E1, E2) and inclusion-rich zones (E9)

(> 4 wt%; at 1000 °C; Fig. 8d). After exploring the effect of varying temperatures (850–1100 °C) in the calculation of the melt MgO contents, we compared our results with previous studies of bulk rock compositions of the host andesite (> 4 wt%; Supplementary Table S2) and enclave (> 2.5 wt%; Supplementary Table S2).

At 1000 ± 50 °C, most intermediate-core zones of type I and II are re-equilibrated with a liquid of lower MgO (< 1 wt%) comparable to the measured compositions of melts inclusions (e.g., MgO 0.5 wt%, Christopher et al. 2014; Supplementary Table S2) and rims in equilibrium with host bulk rock up to 3 wt% and enclave bulk rock up to 5 wt% (Plail 2013; Supplementary Table S2). However, some plagioclase rims of type II appear to be re-equilibrated at 850 °C with a liquid of unrealistically high MgO content (> 6 wt%) compared to the measured compositions of glasses and whole rock samples in the SHV system.

Estimated timescales from diffusion modelling

The diffusive re-equilibration of MgO in melt-plagioclase was modelled for type II plagioclase phenocrysts from the host (at 950 °C) and enclave (at 1050 °C) with an uncertainty of ± 50 °C (Supplementary Table S4). Note that type I profiles were not suitable to be modelled due to the lack of significant change in MgO content between the interior-rim of crystals and the presence of sieve textures and dissolution features. One-stage diffusion models (see “Modelling” section) yielded residence timescales varying from a few hours up to 3 days for plagioclase in the enclave, and on the scale of a few days for phenocrysts in the host. The results of the two-stage diffusion models (Step 1 and 2; see “Modelling” section) vary from a few hours up to 2 days for the intermediate-core plagioclase phenocrysts (Step 1) in equilibrium with enclave melt at 1050 °C (e.g., E1; Fig. 9a), and from 3 to 121 days

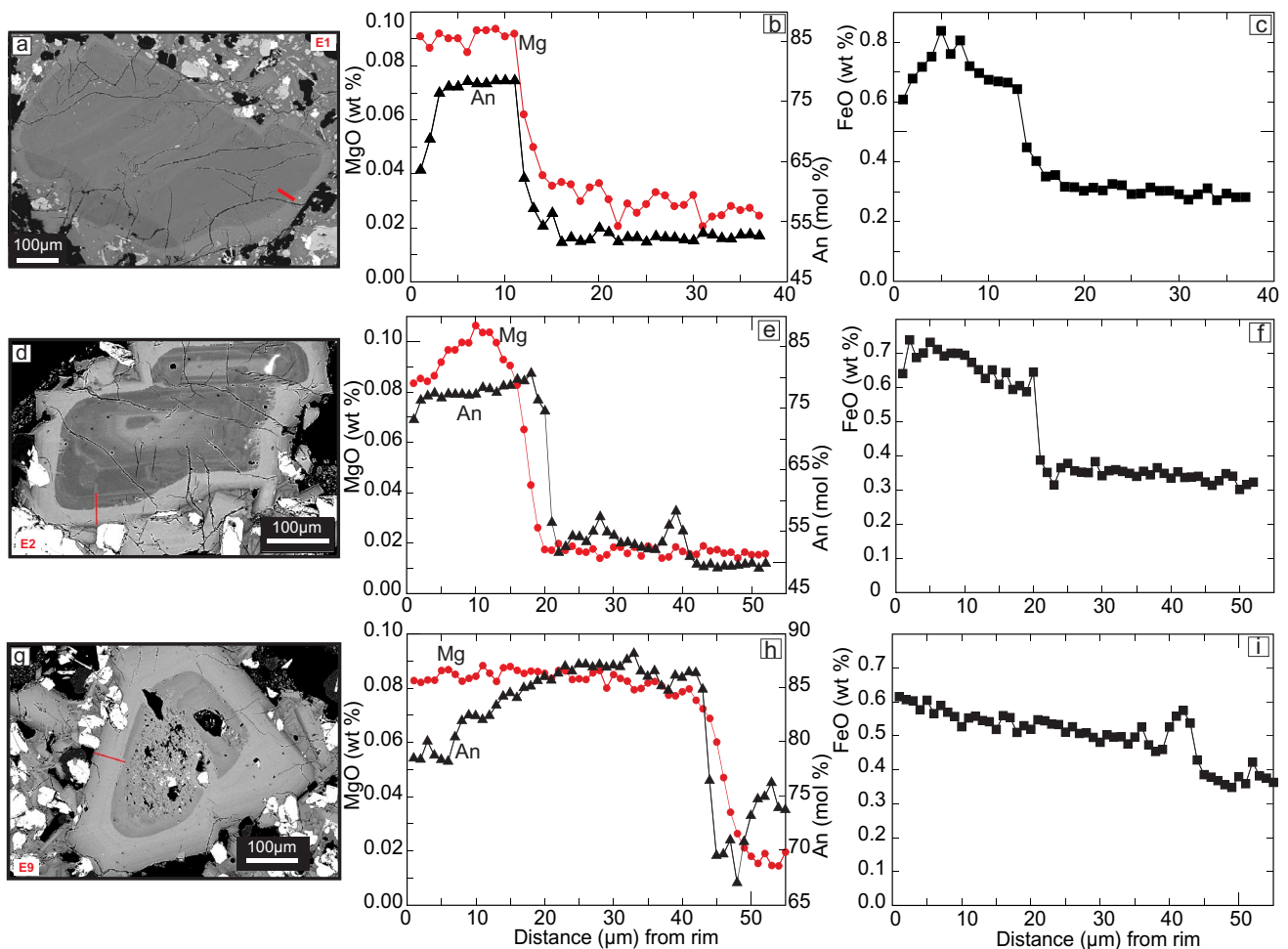


Fig. 7 Examples of BSE images and compositional traverses of plagioclase type I **a** and type II (**d**, **g**) from the andesite host: H6 **a**, H10 **d** and H11 **g**. Red lines mark the position of the electron microprobe

traverse. Phenocrysts show patchy and sodic cores, with a sharp increase in An (black triangle), MgO (red circle) and FeO (black square) contents at their rims

for intermediate-core phenocrysts with host melt at 950 °C (e.g., H10, Fig. 9c). The modelling of the diffusion occurring to the entire plagioclase (interior-rim, Step 2) returned times from a few hours to 5 days for plagioclase phenocrysts found both in the enclave (1050 °C) and host (950 °C; Fig. 9). The uncertainties on the fit model were estimated according to the instrument uncertainties (see Supplementary Information S4) and summarised in Supplementary Table S4 for both one- and two-stage models. However, the two-stage model is considered to be more representative of the actual process that took place than the one-stage model. Running models show that a factor of 1–2 is estimated for the uncertainty in the models due to the temperature variation of ± 50 °C.

Discussion

Magma end-members inferred from plagioclase types, calculated melt compositions and timescales

Textural and compositional features of SHV plagioclase phenocrysts suggest that different crystal zones grew from melts characterised by different composition and/or thermodynamic conditions (e.g., temperature, water in the melt, and pressure). The low An (< 65 mol%) and calculated MgO (< 2 wt%) concentrations of intermediate-core zones of some plagioclases show that they grew

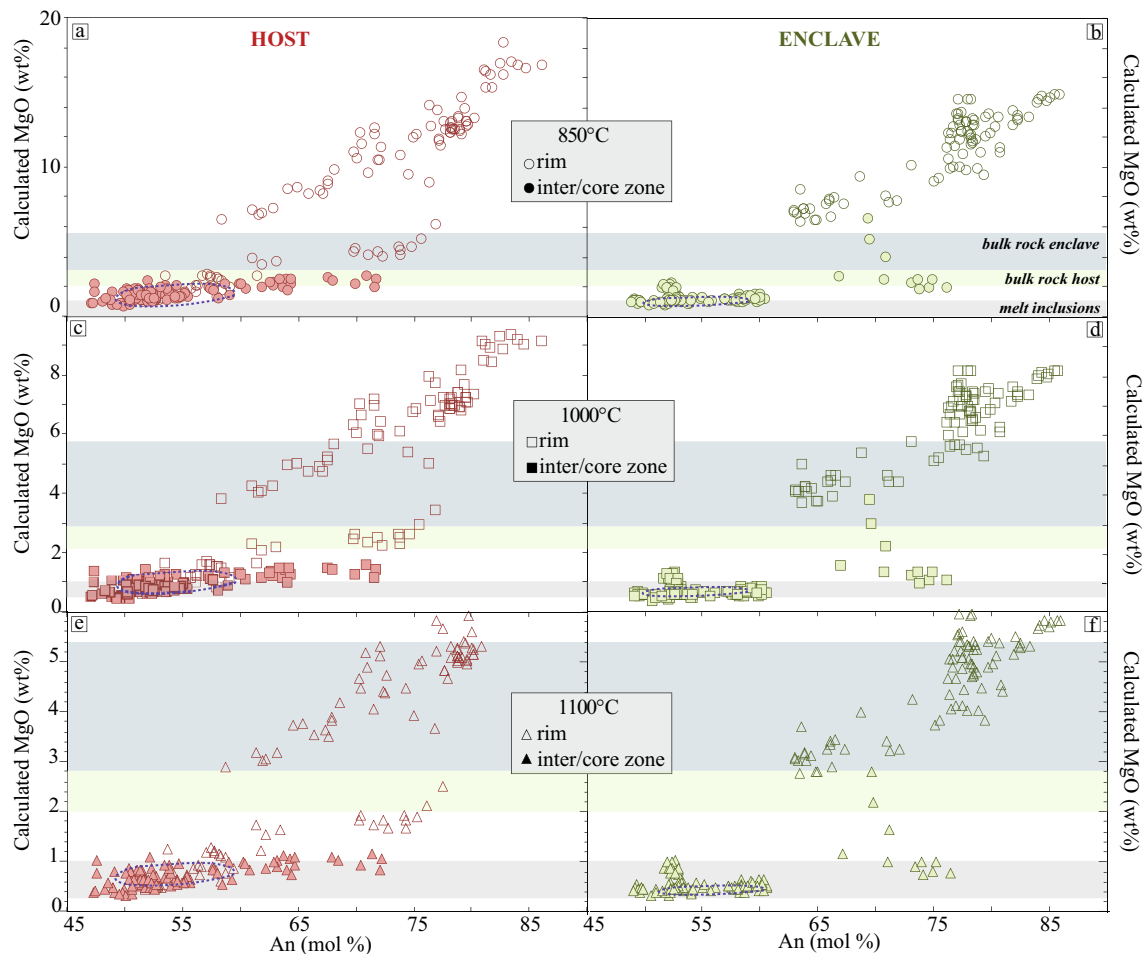


Fig. 8 The calculated MgO-melt concentration in type I (dotted blue line) and type II plagioclase was estimated using Bindeman et al. (1998) for three different temperatures: **a** 850 °C, **b** 1000 °C and, **c** 1100 °C. The dark green bar (from 3 to 6 wt% of MgO) shows the bulk rock composition of the enclaves from previous studies (Phase

I–V). The light green bar, from 2 to 3 wt% MgO is the bulk composition of the host produced during all the phases of the eruption. The light grey bar (from 0 to 1 wt%) shows the concentration of MgO of the melt inclusions trapped in plagioclase as taken from the literature (Christopher et al. 2014; Devine and Rutherford 2014; Plail 2013)

from relatively evolved melts (dacite to rhyolite). Therefore, type I plagioclase phenocrysts represent the melt of the crystal-rich andesitic magma end-member, which crystallised before the intrusion of mafic magma. On the other hand, the overgrowth rims of Type II plagioclase equilibrated with melts of MgO > 2 wt% and their high An content (75 mol%) record the interaction between the andesitic host and the intrusion of mafic magma. The sharp transition (in An and Mg) between intermediate-core and overgrowth rims of type II suggests that changes in the magmatic environment experienced by these crystals were abrupt, and our modelling of diffusive re-equilibration of the Mg supported a time range from a few hours to days before eruption.

Our type I plagioclase, with high An intermediate/core zones within lower An areas are related to the plagioclase

investigated by Zellmer et al. (2003b), which proposed a residence times of up to 300 years between magma heating, remobilization, and eruption using Sr and Ba zoning in plagioclase phenocrysts. Moreover, our type I and II are, respectively, comparable with the classification of type 2 and 3 crystals proposed by Murphy et al. (2000). In their work, plagioclase recorded in their texture processes multiple injections of hotter and mafic magma below andesitic magma that lead to thermal convection and remobilisation of the resident magma (Murphy et al. 2000). However, Murphy et al. (1998) found unzoned and normally zoned plagioclase in rocks from the beginning of the eruption (1995–1997) that we did not find. The lack of these textural types within our sample suggests that the mafic end-member magma was under-saturated in plagioclase. This is consistent with its high-water content (> 7 wt%; Edmonds et al. 2016) that

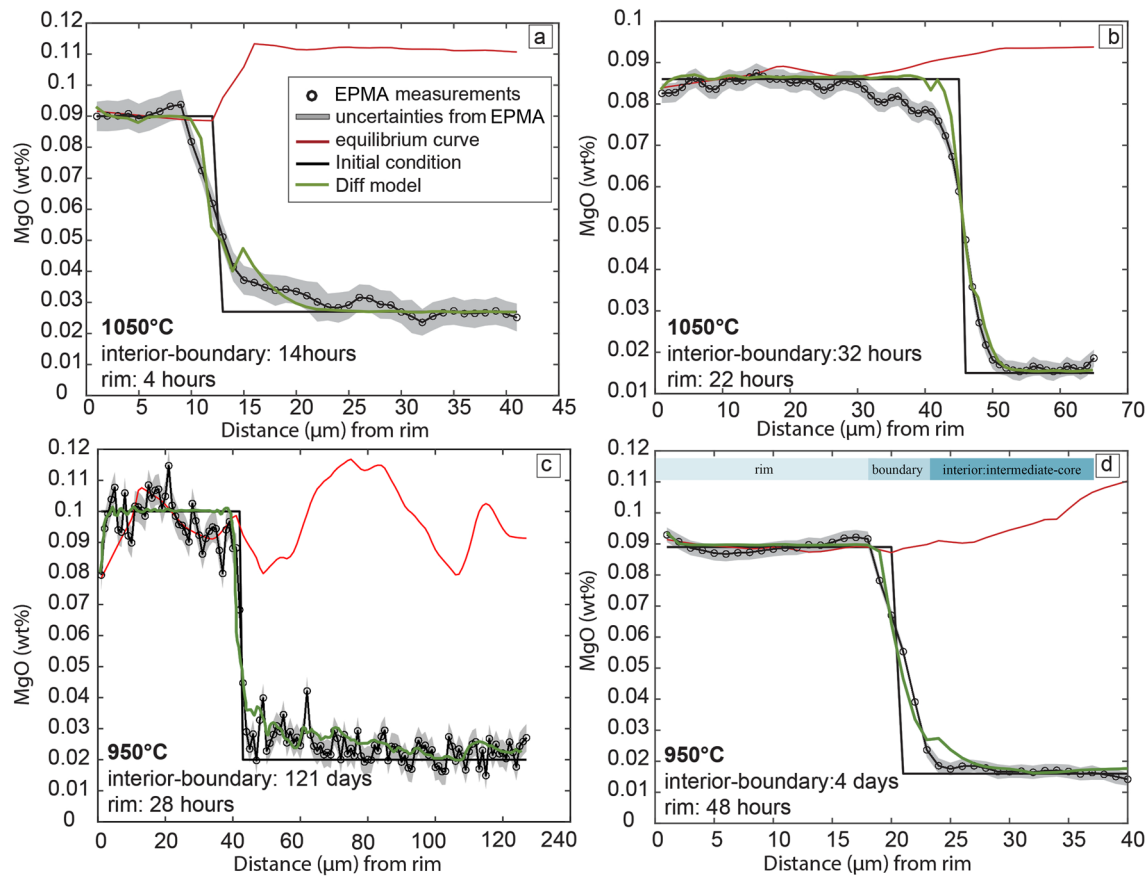


Fig. 9 Diffusion models for type II plagioclase in enclave (a, b) and host (c, d). The black line is the initial condition, calculated on the basis of the anorthite content along the EPMA measurements (black empty circle) with their relative uncertainty (grey area) from EPMA

would have suppressed plagioclase stability. The lack of very high An plagioclase (> 90 mol%) in our sample suggests that plagioclase in the enclaves grew from already more evolved and mixed melts or that the basaltic andesite end-member was close to its liquidus, at about 1050 °C, since it contains only minor pyroxene phenocrysts (e.g., Murphy et al. 1998). This is in accordance with phase equilibria experiments on a basaltic andesite of Mount Pelée, which has a similar composition to the SHV enclaves (Pichavant et al. 2002).

The complexity of magmatic interaction at SHV: intrusion, mixing-hybridization and eruption

To understand mafic–silicic magma interaction it is necessary to constrain the composition and physical properties of the magmatic end-members involved prior to interaction. Type I and II phenocrysts are found both in the host andesite and the basaltic andesite enclave, implying that magmas

instrument. The red continuous line is the equilibrium curve. Results for the two-stage model are shown with a green line. See the text for more details

have exchanged mass as well as heat, and therefore, neither of the erupted rocks have compositions representative of the pre-mingling or mixing magmatic end-members. We identified that the low An content intermediate zone-core of type II plagioclase in the enclave were inherited from the andesitic host. This finding is consistent with previous studies at SHV (Humphreys et al. 2009, 2010; Plail et al. 2014), where magma mingling was shown to result in the exchange and incorporation of phenocrysts and microlites from the andesite into the basaltic andesite enclaves and vice versa. Such observations are common to other volcano case studies (e.g., Mount Pelée; Pichavant et al. 2002) that investigate plagioclase textures and compositions within mixed dacite to basaltic andesite magmas and attests to the dynamic nature of mafic–silicic magma interactions (Feeley and Dungan 1996; Pichavant et al. 2002; Tomiya and Takahashi 2005).

Although in this work we studied the sample from the last eruption Phase (2010), our finding can be linked to the previous processes that are recorded in mineral textures as a series of interactions between coexisting liquids of different

compositions and temperatures that have triggered several cycles of dissolution and regrowth of crystals. The enclave analysed here is representative of the least evolved of enclave types (Type A; Plail et al. 2014), thus a potential cargo of minerals that preserved in their texture the magmatic history.

In the following sections, we show a possible sequence of events preceding and, contemporary to, the interaction between the andesite and intruding basalt, since the eruption started in 1995 until 2010 integrated with previous studies (see Supplementary Fig. S1 for schematic representation).

Andesite and basaltic andesite magmas prior to interaction

Our investigation on mineralogical textures, plagioclase zoning patterns and relative calculated melt compositions indicates that the stored andesite magma was in equilibrium with type I plagioclase, rhyolitic liquid, amphibole and quartz. Thus, before multiple injections of fresh new magmas, a dacite to rhyolite magma was more representative of the host that became andesitic after mixing/hybridisation events. Figure 8a shows that type I plagioclase with An range between 47 and 55 (mol%) are in equilibrium with rhyolite liquid of the host with temperature of 850 °C, which is consistent with experiments of phase equilibria for andesitic host proposed by Couch et al. (2003) and Rutherford and Devine (2003) (Fig. 10). Published studies on melt inclusions in plagioclase phenocrysts and hydrogen concentrations in opx from SHV indicate melt water contents of 4–5 wt% and saturation pressures of 100–130 MPa (Edmonds et al. 2016). At this conditions and temperature of 850 ± 20 °C (Supplementary Figure S1), phase equilibria indicate that the magma would contain > 50% crystals in a rhyolitic liquid similar to the melt

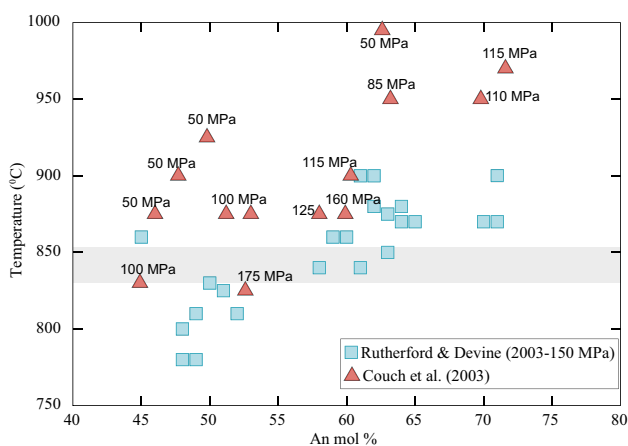


Fig. 10 Temperature and An plagioclase content summarised from the phase equilibrium experiments from Couch et al. (2003) and Rutherford and Devine (2003). The grey field shows the range in host temperature

inclusions (Barclay et al. 1998; Couch et al. 2003; Rutherford and Devine 2003).

Interaction between the host andesite and intruding basalt

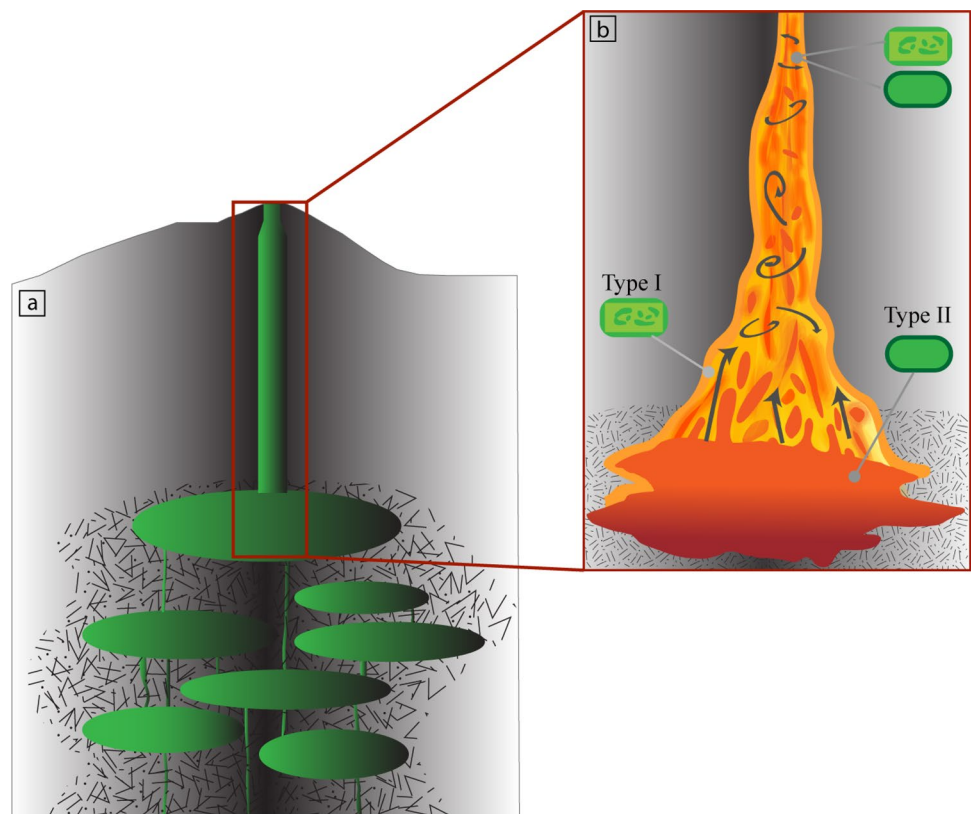
After multiple injections of mafic magma into the shallow plumbing system (Phase I onwards), the crystal-rich host was reheated by intruding basalt, becoming hybrid, while plagioclase (type I and intermediate-core zones of type II) and quartz started to partially dissolve. A hybrid zone developed at the interface between basalt and andesite host, where plagioclase crystals were entrained in the higher temperature/high-Mg intruding, water-rich magma at near liquidus conditions. Such magma could have been generated by fractionation of a more mafic liquid such as the one found in South Soufrière Hills Volcano (Edmonds et al. 2016). Plagioclase partially dissolves and generates a sieve texture, although in some crystals the Mg content increases and re-equilibrates with the mafic magma (Supplementary Figure S1). Amphibole and quartz crystals that were retained in this mafic magma are also resorbed. It is unclear whether the mafic magma was saturated in plagioclase when it came in contact with the andesite or not.

Phase equilibria experiments on a basaltic andesite from neighbouring Mt. Pelée volcano on Martinique Island (Pichavant et al. 2018) show a bulk-rock composition similar to the SHV enclaves. This comparison suggests that the magma would be near its liquidus at 1050 °C and about 8 wt% H₂O, and that with decreasing temperature or water content the first mineral to crystallise is cpx followed by high-An plagioclase. The hydrogen contents of opx in the enclave indicate a higher water content for the enclave than the andesite (about 7 wt% H₂O), and also somewhat higher pressures of 200–300 MPa (Edmonds et al. 2016). Based on these considerations, we propose that the basaltic andesite magma had initially a temperature of 1000–1100 °C and high pressure (200–300 MPa) carrying mainly opx and/or cpx and that most of the plagioclase phenocrysts originated from the andesite by mechanical disaggregation at a later time (Supplementary Figure S1).

Co-eruptive magma interactions

During the last year of eruption (Phase V), more mafic magma (that was partly hybridised) quickly cools, where it is in contact with a larger amount of unheated andesite, triggering crystallisation of high-An rims and producing type II crystals (Fig. 11). These crystals are equilibrated with a liquid with about 5 wt% MgO (i.e., similar to the bulk composition of the enclaves). The modelled re-equilibration of MgO in type II plagioclase yielded time scales varying from hours to up to 2 weeks. Some of the type II crystals from

Fig. 11 Schematic representation of the magmatic plumbing system beneath SHV **a** Detailed mingling and/or mixing processes in the feeding system take place from the magma chamber to the surface **b** The andesite (yellow area) was previously reheated by the intrusion of more mafic magma developing a hybrid layer (red area). Type I plagioclase crystals dissolve and form a sieve texture. Type II crystals are the result of the co-magmatic interaction between magmas that is facilitated by the increase of the interaction surface between magmas due to the change in geometry. Some of the crystals from the enclaves were reincorporated in the andesite magma and vice versa with a consequence exchange in plagioclase types from enclave to andesitic host. For more details see the text



the enclaves are reincorporated into the andesite magma, due to mechanical disaggregation, either during the time of the cooling of the enclaves, or later during high-strain interactions that led to enclave disaggregation as suggested by Humphreys et al. (2009). Most of the type II crystals in the host record the same equilibration experienced by the enclaves with high Mg-liquids, although we did find one example, where partial re-equilibration with the andesite occurred (Fig. 7). The short timescales that we obtained may imply that the mafic–silicic magma interactions occurred syn-eruptive, as also proposed by Plail et al. (2018).

Our investigations suggest that both mafic and silicic magmas coexist at depth with well-defined compositional and thermal identities, rather than forming a fully hybridised magma (Fig. 11b). There is evidence that the magma reservoir below SHV contains both more mafic and silicic magmas as distinct entities (Cashman et al. 2017; Christopher et al. 2015; Paulatto et al. 2019) and that the geometry of the plumbing system changes towards the surface (Costa et al. 2013a; Hautmann et al. 2009). Transition from a magma chamber at about 5 km depth (Costa et al. 2013a; Paulatto et al. 2012, 2019) to a cylindrical conduit at about 1 km depth (Costa et al. 2013a; Paulatto et al. 2012), would force closer interaction between the two magmas. This increased interface could enhance the level of vorticity (Carrara et al. 2020), generating turbulent fluid flows that would allow for very quick and eventual hybridization of the erupted magma.

These conclusions imply that the formation of the enclaves and associated hybridisation are not a direct trigger of the eruption, but rather a consequence of increased turbulence between high contrasting magmas.

Magma interactions at SHV without replenishment of fresh magma

Our results of hour-long timescales are inferred by plagioclase from volcanic rocks erupted during February 2010 (Phase V) suggesting that the overgrowth rim from type II plagioclase is not a consequence of the replenishment of new magma. We harmonised these considerations into the general framework of the entire 1995–2010 eruption integrating previous longer timescale studies on volcanic rock erupted during Phase I (Devine et al. 2003; Zellmer et al. 2003a, b). Therefore, the magmatic system compositionally evolved from Phase I onwards and the recorded history hidden in minerals show multiple injections of more mafic magma and remobilisation on the order of several hundred years (Zellmer et al. 2003b) and several cycles of reheating and remobilisation shortly (days to months) just before the eruption (Devine et al. 2003).

In the final stage (Phase V), the results gained from this study suggest that mafic intrusion was not a driver of eruption and the short timescales (hours-days). Our results indicate that mafic magma was already stored in the upper parts

of the plumbing systems and the injection of fresh magma was interrupted. Indeed, the interruption of fresh magma injection (carrying fresh volatile) into the andesitic host is supported by McGee et al. (2019) and evoked by the progressive ^{210}Pb deficits in the andesite (with the lowest value during Phase II) and the excess of ^{210}Pb in enclaves (with the highest $(^{210}\text{Pb}/^{226}\text{Ra})_0$ ratios in Phase II). Following Plail et al. (2018) the eruption is induced by the destabilisation of the hybrid layer that increased in thickness over time from Phase III until Phase V, without the injection of new magma and led to syn-eruptive enclave formation. Note that if the plagioclase crystals analysed in this work had spent more time in the thicker hybrid layer, we would expect longer times for later erupted plagioclase crystals and not the short timescales obtained in this study. The short time scales that we report rather suggest that the co-eruptive interaction between andesite and basaltic andesite was facilitated by changes in conduit geometry as discussed above (Gottsmann et al. 2020; Hautmann et al. 2009; see “Co-eruptive magma interactions” section).

Conclusion

In this work we offer a novel insight into the final, Phase V, 2010 eruption of SHV through diffusion modelling of Mg zoning patterns in plagioclase crystals. The findings and implications of this work have been integrated with previous studies on the other eruptions phases to provide a wider perspective and more detailed insight into magmatic processes at SHV. The intrusion of mafic magma into the reservoir (Phase I) was proposed as a driver of the eruption (Murphy et al. 2000). Sr and Ba concentration in plagioclase crystals yielded a long timescale (several hundred years) between intruding basalt and remobilisation of andesitic host (Zellmer et al. 2003a, b). However, Fe–Ti zoning in oxides recorded a shorter timescale just before the eruption (days up to few weeks) due to the multiple injections of mafic magma into the shallow reservoir (Devine et al. 2003; Rutherford and Devine 2003).

Despite the presence of enclaves in erupted deposits of each phase of the 1995–2010 SHV eruption (Phases I–V), this work supports a scenario during the final years of the eruption, the intrusion of new magma in the magma chamber ceased (e.g., Plail et al. 2018; McGee et al. 2019). The diffusion modelling of Mg in plagioclase in volcanic rocks from Phase V carried out in this study reveals very short timescales of magmatic interaction prior to eruption, on the order of hours to days. These short timescales, combined with mineralogical textures and calculated melt compositions, point towards a strong efficiency of the co-eruptive mingling/mixing dynamics. We proposed that the interaction of both magma end-members below SHV is facilitated

by favourable fluid-dynamic mixing processes associated with a change in geometry of the plumbing systems, from a wide reservoir to narrow conduit, towards the surface. These geometric changes in the SHV plumbing system have been reported by ground deformation modelling of the crust beneath the volcano (Gottsmann et al. 2020; Hautmann et al. 2009). This study provides additional understanding of SHV from the past to its present state, which may benefit the interpretation of the volcano's monitoring data in future eruption forecasting.

Supplementary Information The online version contains supplementary material available at <https://doi.org/10.1007/s00410-022-01891-z>.

Acknowledgements This work was funded by Macquarie University Research Excellence Scholarship (MQRES) (2015081) associated with an Australian Research Council Discovery Project (DP150100328) awarded to HH, ST and JB. F. Costa acknowledges a National Research Foundation Investigatorship Award (Grant number NRF-NRFI2017-06). We would like to thank Melissa Plail for sharing her sample collection, Steve Craven for the rock preparations, Lilu Cheng and Jason Herrin for their assistance, respectively, during SEM and EPMA analysis. We are grateful to Turker Topal for his help with Matlab code, Benat Oliveira Bravo for helpful discussion about diffusion modelling processes, Lucy McGee and Marthe Klöcking for constructive discussion related to the SHV magmatic system. We thank Alessandro Maini and two anonymous reviewers for their constructive reviews and thank Timothy L. Grove for editorial handling of the manuscript.

Funding Open Access funding enabled and organized by CAUL and its Member Institutions.

Open Access This article is licensed under a Creative Commons Attribution 4.0 International License, which permits use, sharing, adaptation, distribution and reproduction in any medium or format, as long as you give appropriate credit to the original author(s) and the source, provide a link to the Creative Commons licence, and indicate if changes were made. The images or other third party material in this article are included in the article's Creative Commons licence, unless indicated otherwise in a credit line to the material. If material is not included in the article's Creative Commons licence and your intended use is not permitted by statutory regulation or exceeds the permitted use, you will need to obtain permission directly from the copyright holder. To view a copy of this licence, visit <http://creativecommons.org/licenses/by/4.0/>.

References

- Aspinall WP, Miller AD, Lynch LL, Latchman JL, Stewart RC, White RA, Power JA (1998) Soufriere hills eruption, Montserrat, 1995–1997: volcanic earthquake locations and fault plane solutions. *Geophys Res Lett* 25(18):3397–3400. <https://doi.org/10.1029/98gl00858>
- Bacon K, Barnes G (1978) Two-component monolayers IV the excess enthalpies and entropies of mixing in the octadecanol-docosyl sulfate system. *J Colloid Interface Sci* 67(1):70–77
- Barclay J, Rutherford MJ, Carroll MR, Murphy MD, Devine JD, Gardner J, Sparks RSJ (1998) Experimental phase equilibria constraints on pre-eruptive storage conditions of the Soufriere

- hills magma. *Geophys Res Lett* 25(18):3437–3440. <https://doi.org/10.1029/98gl00856>
- Barclay J, Herd RA, Edwards BR, Christopher T, Kiddle EJ, Plail M, Donovan A (2010) Caught in the act: Implications for the increasing abundance of mafic enclaves during the recent eruptive episodes of the Soufriere Hills Volcano, Montserrat. *Geophys Res Lett*. <https://doi.org/10.1029/2010gl042509>
- Bindeman IN, Davis AM, Drake MJ (1998) Ion microprobe study of plagioclase-basalt partition experiments at natural concentration levels of trace elements. *Geochim Cosmochim Acta* 62(7):1175–1193
- Blundy JD, Wood BJ (1991) Crystal-chemical controls on the partitioning of Sr and Ba between plagioclase feldspar, silicate melts, and hydrothermal solutions. *Geochim Cosmochim Acta* 55(1):193–209. [https://doi.org/10.1016/0016-7037\(91\)90411-W](https://doi.org/10.1016/0016-7037(91)90411-W)
- Browne BL, Eichelberger JC, Patino LC, Vogel TA, Dehn J, Uto K, Hoshizumi H (2006a) Generation of porphyritic and equigranular mafic enclaves during magma recharge events at Unzen volcano Japan. *J Petrol* 47(2):301–328. <https://doi.org/10.1093/ptrology/egi076>
- Browne BL, Eichelberger JC, Patino LC, Vogel TA, Uto K, Hoshizumi H (2006b) Magma mingling as indicated by texture and Sr/Ba ratios of plagioclase phenocrysts from Unzen volcano SW Japan. *J Volcanol Geotherm Res* 154(1–2):103–116. <https://doi.org/10.1016/j.jvolgeores.2005.09.022>
- Carrara A, Burgisser A, Bergantz GW (2020) The architecture of intrusions in magmatic mush. *Earth Planet Sci Lett* 549:116539
- Cashman KV, Sparks RSJ, Blundy JD (2017) Vertically extensive and unstable magmatic systems: a unified view of igneous processes. *Science* 355(6331):eaag3055
- Cassidy M, Edmonds M, Watt SFL, Palmer MR, Gernon TM (2015) Origin of basalts by hybridization in andesite-dominated arcs. *J Petrol* 56(2):325–346. <https://doi.org/10.1093/ptrology/egv002>
- Christopher TE, Humphreys MC, Barclay J, Genereau K, De Angelis SM, Plail M, Donovan A (2014) Petrological and geochemical variation during the Soufriere hills eruption, 1995 to 2010. *Geol Soc Lond Mem* 39(1):317–342
- Christopher T, Blundy J, Cashman K, Cole P, Edmonds M, Smith P, Sparks R, Stinton A (2015) Crustal-scale degassing due to magma system destabilization and magma-gas decoupling at Soufrière hills volcano, Montserrat. *Geochim Geophys Geosyst* 16(9):2797–2811
- Clyne MA (1999) A complex magma mixing origin for rocks erupted in 1915, Lassen Peak, California. *J Petrol* 40(1):105–132. <https://doi.org/10.1093/ptrology/40.1.105>
- Costa F, Chakraborty S (2004) Time scales of igneous differentiation obtained from diffusion modeling of compositional zoning in olivine. *Geochim Cosmochim Acta* 68(11):A642–A642
- Costa F, Dungan M (2005) Short time scales of magmatic assimilation from diffusion modeling of multiple elements in olivine. *Geology* 33(10):837–840. <https://doi.org/10.1130/G21675.1>
- Costa F, Chakraborty S, Dohmen R (2003) Diffusion coupling between trace and major elements and a model for calculation of magma residence times using plagioclase. *Geochim Cosmochim Acta* 67(12):2189–2200. [https://doi.org/10.1016/S0016-7037\(00\)01345-5](https://doi.org/10.1016/S0016-7037(00)01345-5)
- Costa F, Dohmen R, Chakraborty S (2008) Time scales of magmatic processes from modeling the zoning patterns of crystals. *Rev Mineral Geochem* 69:545–594. <https://doi.org/10.2138/rmg.2008.69.14>
- Costa A, Wadge G, Stewart R, Odbert H (2013a) Coupled subdaily and multiweek cycles during the lava dome eruption of Soufriere hills volcano Montserrat. *J Geophys Res Solid Earth* 118(5):1895–1903. <https://doi.org/10.1002/jgrb.50095>
- Costa F, Andreastuti S, de Maisonneuve CB, Pallister JS (2013b) Petrological insights into the storage conditions, and magmatic processes that yielded the centennial 2010 Merapi explosive eruption. *J Volcanol Geotherm Res* 261:209–235. <https://doi.org/10.1016/j.jvolgeores.2012.12.025>
- Costa F, Shea T, Ubide T (2020) Diffusion chronometry and the timescales of magmatic processes. *Nat Rev Earth Environ* 1(4):201–214
- Couch S, Sparks RSJ, Carroll MR (2001) Mineral disequilibrium in lavas explained by convective self-mixing in open magma chambers. *Nature* 411(6841):1037–1039. <https://doi.org/10.1038/35082540>
- Couch S, Harford CL, Sparks RSJ, Carroll MR (2003) Experimental constraints on the conditions of formation of highly calcic plagioclase microlites at the Soufriere hills volcano Montserrat. *J Petrol* 44(8):1455–1475. <https://doi.org/10.1093/ptrology/44.8.1455>
- Coussens M, Cassidy M, Watt SFL, Jutzeler M, Tailing PJ, Barfod D, Gernon TM, Taylor R, Hatter SJ, Palmer MR (2017) Long-term changes in explosive and effusive behaviour at andesitic arc volcanoes: chronostratigraphy of the centre hills volcano, Montserrat. *J Volcanol Geotherm Res* 333:15–35. <https://doi.org/10.1016/j.jvolgeores.2017.01.003>
- Davidson JP, Morgan DJ, Charlier BLA, Harlou R, Hora JM (2007) Microsampling and isotopic analysis of igneous rocks: Implications for the study of magmatic systems. *Ann Rev Earth Planet Sci* 35:273–311. <https://doi.org/10.1146/annurev.earth.35.031306.140211>
- Deer WA, Howie RA, Zussman J (1992) An introduction to the rock-forming minerals. Longman Scientific & Technical, UK
- Devine JD, Rutherford MJ (2014) Magma storage region processes of the Soufriere hills volcano, Montserrat. *Geol Soc Mem* 39:361–381. <https://doi.org/10.1144/M39.19>
- Devine JD, Murphy MD, Rutherford MJ, Barclay J, Sparks RSJ, Carroll MR, Young SR, Gardner JE (1998) Petrologic evidence for pre-eruptive pressure-temperature conditions, and recent reheating, of andesitic magma erupting at the Soufriere hills volcano, Montserrat, WI. *Geophys Res Lett* 25(19):3669–3672. <https://doi.org/10.1029/98gl01330>
- Devine JD, Rutherford MJ, Norton GE, Young SR (2003) Magma storage region processes inferred from geochemistry of Fe-Ti oxides in andesitic magma, Soufriere hills volcano, Montserrat, WI. *J Petrol* 44(8):1375–1400. <https://doi.org/10.1093/ptrology/44.8.1375>
- Dohmen R, Blundy J (2014) A predictive thermodynamic model for element partitioning between plagioclase and melt as a function of pressure temperature and composition. *Am J Sci* 314(9):1319–1372. <https://doi.org/10.2475/09.2014.04>
- Druitt TH, Costa F, Deloule E, Dungan M, Scaillet B (2012) Decadal to monthly timescales of magma transfer and reservoir growth at a caldera volcano. *Nature* 482(7383):77–U97. <https://doi.org/10.1038/nature10706>
- Edmonds M, Woods AW (2018) Exsolved volatiles in magma reservoirs. *J Volcanol Geotherm Res* 368:13–30
- Edmonds M, Kohn SC, Hauri EH, Humphreys MCS, Cassidy M (2016) Extensive, water-rich magma reservoir beneath southern Montserrat. *Lithos* 252:216–233. <https://doi.org/10.1016/j.lithos.2016.02.026>
- Edmonds M, Cashman KV, Holness M, Jackson M (2019) Architecture and dynamics of magma reservoirs. *Philos Trans R Soc Math Phys Eng Sci* 377(2139):20180298. <https://doi.org/10.1098/rsta.2018.0298>
- Eichelberger JC (1980) Vesiculation of mafic magma during replenishment of silicic magma reservoirs. *Nature* 288(5790):446–450. <https://doi.org/10.1038/288446a0>
- Fabbro GN, Druitt TH, Costa F (2017) Storage and eruption of silicic magma across the transition from dominantly effusive to

- caldera-forming states at an Arc volcano (Santorini, Greece). *J Petrol* 58(12):2429–2464. <https://doi.org/10.1093/petrology/egy013>
- Fabbro GN, McKee CO, Sindang ME, Eggins S, de Maisonneuve CB (2020) Variable mafic recharge across a caldera cycle at Rabaul, Papua New Guinea. *J Volcanol Geotherm Res* 393:106810
- Feeley TC, Dungan MA (1996) Compositional and dynamic controls on mafic-silicic magma interactions at continental arc volcanoes: evidence from Cordón El Guadal, Tatará San Pedro complex, Chile. *J Petrol* 37(6):1547–1577. <https://doi.org/10.1093/petrology/37.6.1547>
- Flaherty T, Druitt T, Tuffen H, Higgins MD, Costa F, Cadoux A (2018) Multiple timescale constraints for high-flux magma chamber assembly prior to the late bronze age eruption of Santorini (Greece). *Contrib Mineral Petrol* 173(9):1–21
- Gottsmann J, Flynn M, Hickey J (2020) The transcrustal magma reservoir beneath Soufrière hills volcano Montserrat: insights from 3-D geodetic inversions. *Geophys Res Lett*. <https://doi.org/10.1029/2020GL089239>
- Grove TL, Baker MB, Kinzler RJ (1984) Coupled CaAl-NaSi diffusion in plagioclase feldspar: experiments and applications to cooling rate speedometry. *Geochim Cosmochim Acta* 48(10):2113–2121
- Harford CL, Pringle MS, Sparks RSJ, Young SR (2002) The volcanic evolution of Montserrat using $^{40}\text{Ar}/^{39}\text{Ar}$ geochronology. *Geol Soc Lond Mem* 21(1):93–113. <https://doi.org/10.1144/gsl.mem.2002.021.01.05>
- Hautmann S, Gottsmann J, Sparks RSJ, Costa A, Melnik O, Voight B (2009) Modelling ground deformation caused by oscillating overpressure in a dyke conduit at Soufrière Hills Volcano Montserrat. *Tectonophysics* 471(1–2):87–95
- Holness MB, Stock MJ, Geist D (2019) Magma chambers versus mush zones: constraining the architecture of sub-volcanic plumbing systems from microstructural analysis of crystalline enclaves. *Phil Trans R Soc A* 377(2139):20180006
- Humphreys MCS, Christopher T, Hards V (2009) Microlite transfer by disaggregation of mafic inclusions following magma mixing at Soufrière Hills Volcano Montserrat. *Contrib Mineral Petrol* 157(5):609–624. <https://doi.org/10.1007/s00410-008-0356-3>
- Humphreys MCS, Edmonds M, Christopher T, Hards V (2010) Magma hybridisation and diffusive exchange recorded in heterogeneous glasses from Soufrière Hills Volcano, Montserrat. *Geophys Res Lett* 37
- Kahl M, Chakraborty S, Costa F, Pompilio M, Liuzzo M, Viccaro M (2013) Compositionally zoned crystals and real-time degassing data reveal changes in magma transfer dynamics during the 2006 summit eruptive episodes of Mt. Etna. *Bull Volcanol* 75(2). <https://doi.org/10.1007/s00445-013-0692-7>
- Kent AJR, Darr C, Koleszar AM, Salisbury MJ, Cooper KM (2010) Preferential eruption of andesitic magmas through recharge filtering. *Nat Geosci* 3(9):631–636. <https://doi.org/10.1038/Ngeo924>
- Komorowski JC, Legendre Y, Christopher T, Bernstein M, Stewart R, Joseph E, Fournier N, Chardot L, Finizola A, Wadge G, Syers R, Williams C, Bass V (2010) Insights into processes and deposits of hazardous vulcanian explosions at Soufrière Hills Volcano during 2008 and 2009 (Montserrat, West Indies). *Geophys Res Lett*. <https://doi.org/10.1029/2010gl042558>
- Longpre MA, Stix J, Costa F, Espinoza E, Munoz A (2014) Magmatic processes and associated timescales leading to the January 1835 eruption of Cosiguina Volcano, Nicaragua. *J Petrol* 55(6):1173–1201. <https://doi.org/10.1093/petrology/egu022>
- Mann CP (2010) Magma chamber dynamics at Soufrière Hills volcano, Montserrat. PhD thesis, McGill University
- McGee L, Reagan M, Handley H, Turner S, Sparks RS, Berlo K, Barclay J, Turner M (2019) Volatile behaviour in the 1995–2010 eruption of the Soufrière Hills Volcano, Montserrat recorded by U-series disequilibria in mafic enclaves and andesite host. *Earth Planet Sci Lett* 524:115730
- McGee L, Reagan M, Turner S, Sparks RS, Handley H, Didonna R, Berlo K, Hansen S, Barclay J (2021) U-series histories of magmatic volatile phase and enclave development at Soufrière Hills Volcano Montserrat. *Chem Geol* 559:119957
- Morgan D, Blake S, Rogers N, DeVivo B, Rolandi G, Macdonald R, Hawkesworth C (2004) Time scales of crystal residence and magma chamber volume from modelling of diffusion profiles in phenocrysts: Vesuvius 1944. *Earth Planet Sci Lett* 222(3–4):933–946
- Murphy MD, Sparks RSJ, Barclay J, Carroll MR, Lejeune AM, Brewer TS, Macdonald R, Black S, Young S (1998) The role of magma mixing in triggering the current eruption at the Soufrière Hills Volcano, Montserrat, West Indies. *Geophys Res Lett* 25(18):3433–3436. <https://doi.org/10.1029/98gl00713>
- Murphy MD, Sparks RSJ, Barclay J, Carroll MR, Brewer TS (2000) Remobilization of andesite magma by intrusion of mafic magma at the Soufrière Hills Volcano, Montserrat, West Indies. *J Petrol* 41(1):21–42. <https://doi.org/10.1093/petrology/41.1.21>
- Oldenburg CM, Spera FJ, Yuen DA, Sewell G (1989) Dynamic mixing in magma bodies—theory, simulations, and implications. *J Geophys Res Solid* 94(B7):9215–9236. <https://doi.org/10.1029/JB094iB07p09215>
- Paulatto M, Annen C, Henstock TJ, Kiddle E, Minshull TA, Sparks R, Voight B (2012) Magma chamber properties from integrated seismic tomography and thermal modeling at Montserrat. *Geochim Geophys Geosyst*. <https://doi.org/10.1029/2011GC003892>
- Paulatto M, Moorkamp M, Hautmann S, Hooft E, Morgan JV, Sparks RSJ (2019) Vertically extensive magma reservoir revealed from joint inversion and quantitative interpretation of seismic and gravity data. *J Geophys Res Solid Earth* 124(11):11170–11191
- Pichavant M, Martel C, Bourdier JL, Scaillet B (2002) Physical conditions, structure, and dynamics of a zoned magma chamber: Mount Pelee (Martinique, Lesser Antilles Arc). *J Geophys Res Solid Earth* 107(B5). <https://doi.org/10.1029/2001jb000315>
- Pichavant M, Poussineau S, Lesne P, Solaro C, Bourdier J-L (2018) Experimental parametrization of magma mixing: application to the AD 1530 eruption of La Soufrière, Guadeloupe (Lesser Antilles). *J Petrol* 59(2):257–282. <https://doi.org/10.1093/petrology/egy030>
- Plail M (2013) Geochemical and petrological investigation into the magmatic system at Soufrière Hills Volcano, Montserrat. PhD Thesis. University of East Anglia
- Plail M, Barclay J, Humphreys MCS, Edmonds M, Herd RA, Christopher TE (2014) Characterization of mafic enclaves in the erupted products of Soufrière Hills Volcano, Montserrat, 2009 to 2010. *Geol Soc Mem* 39:343–360. <https://doi.org/10.1144/M39.18>
- Plail M, Edmonds M, Woods AW, Barclay J, Humphreys MCS, Herd RA, Christopher T (2018) Mafic enclaves record syn-eruptive basalt intrusion and mixing. *Earth Planet Sci Lett* 484:30–40. <https://doi.org/10.1016/j.epsl.2017.11.033>
- Putirka KA (2005) Igneous thermometers and barometers based on plagioclase plus liquid equilibria: tests of some existing models and new calibrations. *Am Mineral* 90(2–3):336–346. <https://doi.org/10.2138/am.2005.1449>
- Rutherford MJ, Devine JD (2003) Magmatic conditions and magma ascent as indicated by hornblende phase equilibria and reactions in the 1995–2002 Soufrière Hills magma. *J Petrol* 44(8):1433–1454. <https://doi.org/10.1093/petrology/44.8.1433>
- Ryan GA, Loughlin SC, James MR, Jones LD, Calder ES, Christopher T, Strutt MH, Wadge G (2010) Growth of the lava dome and extrusion rates at Soufrière Hills Volcano, Montserrat, West Indies: 2005–2008. *Geophys Res Lett*. <https://doi.org/10.1029/2009gl041477>

- Scaillet B, Whittington A, Martel C, Pichavant H, Holtz F (2000) Phase equilibrium constraints on the viscosity of silicic magmas II: implications for mafic-silicic mixing processes. *Trans Roy Soc Edinburgh Earth* 91:61–72. <https://doi.org/10.1017/S026359330000729x>
- Scarlato P, Mollo S, Petrone CM, Ubide T, Di Stefano F (2021) Interpreting magma dynamics through a statistically refined thermometer: implications for clinopyroxene Fe–Mg diffusion modeling and sector zoning at stromboli. In: *Crustal magmatic system evolution: anatomy, architecture, and physico-chemical processes*, pp 195–212
- Sparks R, Marshall L (1986) Thermal and mechanical constraints on mixing between mafic and silicic magmas. *J Volcanol Geotherm Res* 29(1–4):99–124
- Sparks RJ, Sigurdsson H, Wilson L (1977) Magma mixing—mechanism for triggering acid explosive eruptions. *Nature* 267(5609):315–318. <https://doi.org/10.1038/267315a0>
- Sparks RSJ, Murphy MD, Lejeune AM, Watts RB, Barclay J, Young SR (2000) Control on the emplacement of the andesite lava dome of the Soufriere Hills volcano Montserrat by degassing-induced crystallization. *Terra Nova* 12(1):14–20
- Spera FJ, Yuen DA, Kirschvink SJ (1982) Thermal boundary layer convection in silicic magma chambers: effects of temperature-dependent rheology and implications for thermogravitational chemical fractionation. *J Geophys Res Solid Earth* 87(B10):8755–8767
- Tomiya A, Takahashi E (2005) Evolution of the magma chamber beneath Usu volcano since 1663: a natural laboratory for observing changing phenocryst compositions and textures. *J Petrol* 46(12):2395–2426. <https://doi.org/10.1093/petrology/egi057>
- Trial AF, Spera FJ (1990) Mechanisms for the generation of compositional heterogeneities in magma chambers. *Geol Soc Am Bull* 102(3):353–367. [https://doi.org/10.1130/0016-7606\(1990\)102%3c0353:Mftgoc%3e2.3.Co;2](https://doi.org/10.1130/0016-7606(1990)102%3c0353:Mftgoc%3e2.3.Co;2)
- Ubide T, Neave DA, Petrelli M, Longpré M-A (2021) Crystal archives of magmatic processes. *Front Earth Sci* 722
- Van Orman JA, Cherniak DJ, Kita NT (2014) Magnesium diffusion in plagioclase: dependence on composition, and implications for thermal resetting of the Al-26-Mg-26 early solar system chronometer. *Earth Planet Sci Lett* 385:79–88. <https://doi.org/10.1016/j.epsl.2013.10.026>
- Wadge G, Voight B, Sparks RSJ, Cole PD, Loughlin SC, Robertson REA (2014) An overview of the eruption of Soufriere Hills Volcano, Montserrat from 2000 to 2010. *Geol Soc Mem* 39:1–39. <https://doi.org/10.1144/M39.1>
- Young SR, Sparks RSJ, Aspinall WP, Lynch LL, Miller AD, Robertson REA, Shepherd JB (1998) Overview of the eruption of Soufriere Hills Volcano, Montserrat, 18 July 1995 to December 1997. *Geophys Res Lett* 25(18):3389–3392. <https://doi.org/10.1029/98GL01405>
- Zellmer GF, Hawkesworth CJ, Sparks RSJ, Thomas LE, Harford CL, Brewer TS, Loughlin SC (2003a) Geochemical evolution of the Soufriere Hills Volcano, Montserrat lesser Antilles volcanic arc. *J Petrol* 44(8):1349–1374. <https://doi.org/10.1093/petrology/44.8.1349>
- Zellmer GF, Sparks RSJ, Hawkesworth CJ, Wiedenbeck M (2003b) Magma emplacement and remobilization timescales beneath Montserrat: insights from Sr and Ba zonation in plagioclase phenocrysts. *J Petrol* 44(8):1413–1431. <https://doi.org/10.1093/petrology/44.8.1413>

Publisher's Note Springer Nature remains neutral with regard to jurisdictional claims in published maps and institutional affiliations.